A Study on Aluminum Pad Large Deformation during Copper Wirebonding for High Power IC Package

Hsiang-Chen Hsu[1,2,*], Shaw-Yuan Wang[1], and Li-Ming Chu[3,4]

[1]Department of Mechanical and Automation Engineering, I-Shou University, Kaohsiung, Taiwan, ROC.

[2]Department of Industrial management, I-Shou University, Kaohsiung, Taiwan, ROC.

[3]Interdisciplinary Program of Green and Information Technology, National Taitung University, Taitung, Taiwan, ROC.

[4]Department of Applied Science, National Taitung University, Taitung, Taiwan, ROC.

Abstract

In this paper, a 3-D finite element prediction on aluminum pad squeeze during the copper wire bonding process for high power IC package is presented. ANSYS Parametric Design Language (APDL) has been implemented on modelling, mesh density, boundary condition (BC), impact stage and contact mode for the first bond process. The ANSYS/LS-DYNA solver is applied to solve dynamics and LS-PREPOST is used to observe the predicted large plastic deformation on bond pad and stress on microstructure under pad. In view of high power IC package, larger diameter of copper wire is required for electric loading for its low cost. In this research, a large diameter of 2 mil (50 um) uncoated pure copper (4N) wire is applied to simulate first bond impact-contact process. As the scale double enlarged, the problems encountered in simulation are usually evident. Preliminary results on impact stage demonstrate that negative volume/hourglass on large distortion can be solved by tune-up inertial contact settings and mesh density. However, sever hourglass defect would occur on ultrasonic stage and remain a pending problem. A series of prediction has been conducted on the first bond process during impact stage and the results can then be applied to the dynamic wirebonding assembly process.
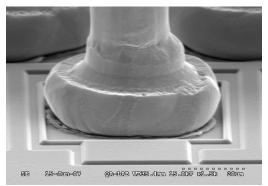
Keywords: copper wirebonding, large plastic deformation, impact-contact, hourglass defect

1. Introduction

Although several advanced interconnection techniques have been developed recently [1-3], the wire bonding process is still widely used in semiconductor packaging industries for its easy application and low cost. Thermosonic bonding (T/S bonding) technique [4] has shown better reliability and good interconnection among all wirebonding processes. The 4N (99.99%) thin gold wire (1mil diameter) is commonly used in wirebonding process because it has mechanically good elongation and electrically low resistivity [5]. Bonding wire usually divided into three different zones, namely free air ball (FAB), HAZ (heat affected zone) and as-drawn wire due to the effect of EFO (electric flame-off). The material behavior of three zones in gold wire has been fully investigated by many earlier works [5-6]. However, elastic modulus (E) and Poisson's ratio (υ) at leveled working temperature for FAB and HAZ on gold wire as well as Cu wire are still scarcely known. The micro-Vickers indentation test was applied to obtain the Vickers hardness (HV) and then transfer to ultimate tensile stress (UTS). While the surface tensile strength can be determined by Nano-indentation test. The thermo-tensile mechanical attributes were measured by our self-designed pull test fixture.

---

* Corresponding author. E-mail address: hchsu@isu.edu.tw

As the price of gold (Au) increases, the substitute material was focused on Pd-coated Cu wire or bare Cu wire just for cost down. The Aluminum (Al) pad has been replaced by Al-Cu pad in accordance with Cu material property in the wire bonding process. It is also an excellent replacement for Au wire due to its similar electrical properties. Self inductance and self capacitance are nearly the same for Au and Cu wire. However, the higher rigidity and more hardness [6-7] results in easily squeeze out the bond pad around the smashed ball, as shown in Fig. 1. Another issue is more bonding power and higher working temperature required in Cu wire bonding process. The dielectric material in circuit under pad (CUP) for wafer technology node (<60 nm) is low-k material and for wafer technology node (<28 nm) is ultra low-k material. Because the low-k/ultra low-k material (nano-porous silicon oxide) is brittle, Copper wirebonding process easily damaged the inter-metal dielectric (IMD) layer, which is demonstrated in Fig. 2.
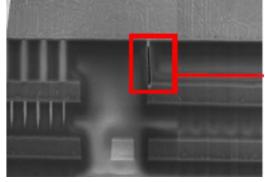

Fig. 1 Large deformation and squeeze out bond pad near ball bond [8]

Fig. 2 Micro cracks occurred in IMD layer beneath the bond pad [8]

Another advantage of Cu wire is lower resistivity. Hence, Cu wire is a very common interconnected media used for high power transmission. Although ultra-thin diameter of wire (0.8 mil (20 μm)) has been applied to ASIC IC or memory IC, large diameter of copper wire (2 mil (50 μm)) is still used on high power IC. Size effects for larger diameter are visible. Reliability on bond pad squeeze and CUP micro-crack are much more overt. These attract many researchers and scholar attention on copper wire high power IC package.

Because the complete mechanism of the wire bonding process includes z-motion, impact and ultrasonic vibration stages [9-10], many material properties of bond wire were scarcely realized. The wirebonding is therefore essentially difficult to simulate by numerical approach. Few papers [11-12] published the reliability of wirebonding process using finite element analysis (FEA) software ANSYS/LS-DYNA. However, some of the bonding material data in these papers were numerical assumption. With sufficient experimental material properties obtained in this research, both 2D and 3D FEA models were developed to predict the dynamic response of the wire bonding process.

2. Experimental Works

Tensile mechanical properties of thin 4N Au wire and Cu wire before/after EFO (electrical flame-off) have been investigated by self-design pull test fixture. Microstructure characteristics of FAB and HAZ are also carefully examined. The mechanical tensile properties for such ultra-thin wire are difficultly evaluated in traditional pull test. Hence, microtensile tests have been carried out by employing the Instron-3365 universal test system with 5N±0.5% load cell and self-designed pull test fixtures. Thermal effects (25, 125 and 200°C) on material properties are taken into account. The chamber needs to be specially processed with Nitrogen gas to avoid oxidization for Cu wire. It has been reported that the plastic behavior and fracture will occur in the HAZ area when external loading is applied. It is, therefore, clear that the breakage sites of EFO wire are in the neck somewhere between HAZ and FAB. Fig. 3 schematically illustrates the self-designed pull test fixtures for the HAZ.
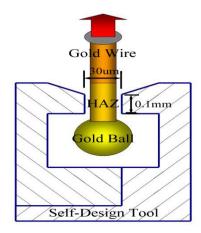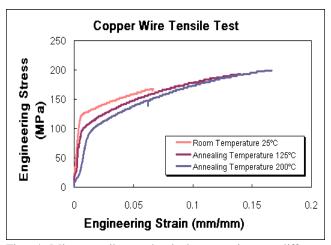
Fig. 3 Self-designed tensile test fixtures for the neck (HAZ)

2.1. Micro mechanical tensile test

Fig. 4 and Fig. 5 show the temperature effects on stress-strain curves for as-drawn and EFO bare Cu wire.
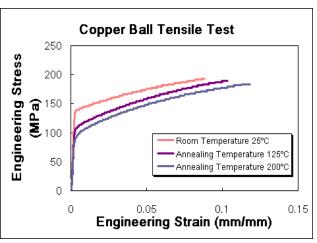

Fig. 4 Micro-tensile mechanical properties at different temperature for as-drawn bare Cu wire

Fig. 5 Micro-tensile mechanical properties at different temperature for EFO bare Cu wire

True stress-strain (σ_T - ε_T) relationships from plastic deformation to necking can be evaluated from engineering stress-strain curves (σ - ε). By power law in Eq. (1),

$$\sigma_T = K\varepsilon_T^n \tag{1}$$

where n is the hardening index and K is the coefficient of strength. The value of hardening index is $0 \leq n \leq 1$ which is shown to be a key factor for FEA simulation. Taking logarithm on both sides

$$\log \sigma_T = \log K + n \log \varepsilon_T \tag{2}$$

$$n = \frac{d(\log \sigma)}{d(\log \varepsilon)} = \frac{\log(\sigma_J) - \log(\sigma_i)}{\log(\varepsilon_J) - \log(\varepsilon_i)} = \frac{\varepsilon}{\sigma} \frac{d\sigma}{d\varepsilon} \tag{3}$$

For strain-rate effect,

$$\sigma_T = K\dot{\varepsilon}^m \tag{4}$$

$$m = \left(\frac{\partial \ln \sigma_T}{\partial \ln \dot{\varepsilon}} \right)_{\varepsilon,T} = \frac{\dot{\varepsilon}}{\sigma} \left(\frac{\partial \sigma_T}{\partial \dot{\varepsilon}} \right)_{\varepsilon,T} = \frac{\Delta \log \sigma}{\Delta \log \dot{\varepsilon}} = \frac{\log \sigma_{T2} - \log \sigma_{T1}}{\log \dot{\varepsilon}_2 - \log \dot{\varepsilon}_1} = \frac{\log(\sigma_{T2}/\sigma_{T1})}{\log(\dot{\varepsilon}_2/\dot{\varepsilon}_1)} \tag{5}$$

From the above figures, true stress-strain mechanical properties in this study is listed in Table 1, where E is Young's modulus, σ_Y is yield strength, TS is tensile strength and ε^F is failure strain. From equation (2), hardening index n and coefficient of strength K can be quickly determined as 408 MPa.

Table 1 True stress-strain mechanical properties

Material	Density (g/cm³)	Poisson's Ratio	Young's Modulus(Gpa)	Yield Stress (Mpa)	Tangent Modulus (Gpa)	Elongation (%) ε^n
Copper Ball (200℃)	19.3	0.43	30	110	0.30	12
Al-Pad	2.71	0.33	69	400	1.38	13
Passivation	1.31	0.24	32	350	3.20	3
Low-k IMD	2.00	0.30	18	80	1.80	3
Copper Via	8.91	0.38	121	330	0.60	3
Oxide	2.64	0.32	66	430	6.60	3
USG	2.00	0.23	80	380	8.00	3
Al-Cu Pad	2.85	0.31	100	400	610	0.054
Die	2.33	0.23	161	-	-	

2.2. Finite element prediction

Both 2-D and 3-D finite element models based on FEA software ANSYS/LS-DYNA codes are developed to simulate the wirebonding process. The geometry of the overall structure was first built to create models. Since FEA prediction also focuses on the strain/stress beneath the bond pad, the entire microstructure of Cu/low-k layer should be well defined. Fig. 6 and Fig. 7 present the 2D FEA geometry, microstructure of Cu/low-k IMD and 3D FEA solid model, respectively.

Because the accurate material properties should be reflected as inputs for precise finite element analysis, the above experimental measured data can then be directly applied to the existing FEA model. A fine mesh scheme is required to evaluate large plastic deformations on mashed FAB with a sufficient accuracy. It should be noted that the small contact region between capillary and FAB is always collapsed, which resulted in the so-called hourglass mesh or zig-zag patch during iteration approach. This happens on hexahedral 3D solid reduced integration elements in FEA model and needed to be re-meshed very frequently. In addition, the precise dimension for FEA model should be carefully measured. Table 2 lists the modal cart of capillary (tool) and Table 3 specifies the dimension of Cu/low-k IMD microstructure beneath the bond pad. The diameter of Cu wire is 50 μm and 85 μm of FAB (free air ball).
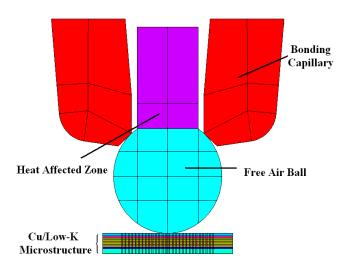

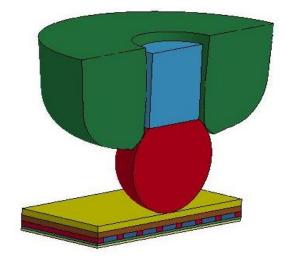Fig. 6 Finite element 2D copper wirebonding model.

Fig. 7 Finite element 3D copper wirebonding model.

Table 2 Detail charts for capillary

Descriptions	Dimensions	Diagram of Capillary
Tip Diameter (T)	188um	
Hole Diameter (H)	58um	
Chamfer Diameter (B)	81um	
Inside Chamfer (IC)	11um	
Inside Chamfer Angle (CA)	90°	
Face Angle (FA)	22°	
Outside Radius (OR)	38um	

Table 3 Detail dimension for microstructure beneath the bond pad

	Length(um)	Width(um)	Height(um)
Pad	146	73	5.2
Passivation	146	73	4.58
Low-k IMD	146	73	4
Copper Via	14	14	4
Oxide	146	73	1.8
Die	146	73	1.8

2.3. Physical mechanism

The bonding process is simulated in three steps. In the first step, the capillary (also refer to the "tool") push FAB downward 10 μm within 0.7 ms to touch the pad. Second, the tool is continuously pushing FAB impact pad and the contact face/length between ball and pad became welded. The third step provides a slightly downward force and ultrasonic vibration, which refers to 120 kHz frequency, 1 μm amplitude within 4 ms vibration time. Loading for the tool is: (1) y-travel and impact time is 0.3 ms, (2) the vertical displacement is 36 μm, (3) the horizontal displacement is 2 μm. Fig. 8 demonstrates the key physical mechanism in wirebonding process
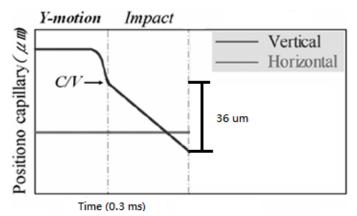
Fig. 8 Capillary displacement physical mechanism

2.4. Boundary conditions

All the boundary conditions based on the wirebonding physical process for 3D predicted FEA model are illustrated in Fig. 9. The bottom surface of FEA model is assumed to be fixed.
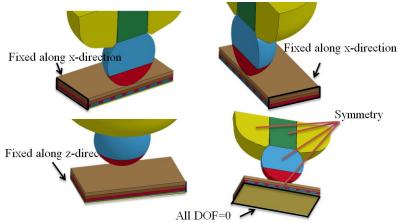
Fig. 9 Boundary conditions for the predicted 3D FEA model

3. Result and Discussion
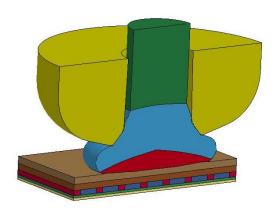
3.1. Squeeze-out bond pad

Fig. 10 FEA predicted wirebonding model

Larger plastic deformation occurred in the area under smashed FAB. Fig. 10 displays the predicted results for FEA wirebonding model. As can be seen, the largest deformation took place in 2 regions: (1) contact area between capillary and FAB, and (2) contact area between FAB and bond pad. Negative volume, zig-zag patch and hourglass elements are always happening and producing meaningless results during numerical iterations. Mesh density and element shape in the largest deformation regions are particularly addressed to avoid numerical iteration errors. Squeeze-out bond pad can be controlled by giving the optimal conditions in FEA model. Fig. 11 presents the predicted maximum squeeze-out bond pad.
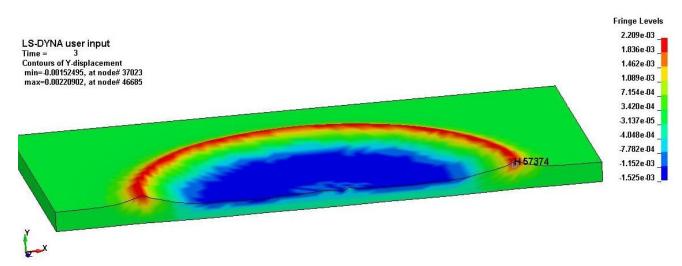

Fig. 11 Predicted maximum squeeze-out bond pad

3.2. Predicted effective stress

Once the bond pad squeeze has been optimized, special attentions are focused on the dynamic response beneath the bond pad. Fig. 12 shows the predicted effective stress vs. time history in low-k IMD layers and the predicted effective stress contours is shown in Fig. 13.
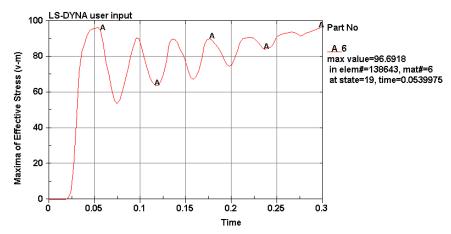

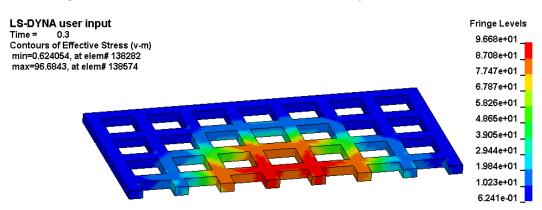Fig. 12 Predicted maximum effective stress vs. time history in low-k microstructure

Fig. 13 Predicted maximum effective stress at the end of impact motion

3.3. Parametric studies

An increase in the bond pad would result in a decrease both in the maximum effective stress in the bond pad and the squeeze-out bond pad. On the contrary, an increase in the bond pad would result in an increase in the maximum effective stress in the low-k IMD microstructure. Table 4 lists predicted results as the bond pad height is increased.

Table 4 Predicted maximum effective stress for different bond heights.

Bond Pad Height (μm)	5.2	6.2	7.2
Maximum Effective Stress (Mpa) on Bond Pad	131	111	109
Squeeze-out Bond Pad (μm)	2.22	1.44	1.34
Maximum Effective Stress (Mpa) in Low-k IMD	96.69	96.76	98.88

4. Conclusions

In this paper, the predicted copper wirebonding process for high power IC based on FEA model has been developed. The insight of the physical mechanism of wirebonding process has also been explored. The experiment works on micro mechanical tensile test and true stress-strain relationships for Cu wire have been determined. With these material properties, the FEA predicted wirebonding model becomes feasible and numerical simulation errors have been fixed in this research. Parametric study reveals an increase in the bond pad height would reduce the large plastic deformation as well as the maximum effective stress on the bond pad. The predicted results can be directly applied to the practical assembly process.

References

[1] Y. J. Lin, C. Kang, L. Chua, W. K. Choi, and S. W. Yoon, "Advanced 3D eWLB-PoP (embedded wafer level ball grid array-package on package) technology," Proc. 66th Electronic Components and Technology Conference, May 2016, pp. 1772-1777.

[2] M. C. Hsieh, K. T. Kang, H. C. Choi, and Y. C. Kim, "Thin profile flip chip package-on-package development," Proc. 11th International Microsystems, Packaging, Assembly and Circuits Technology Conference, October 2016, pp. 143-147.

[3] N. Srikanth, S. Murali, Y. M. Wong, and C. J. Vath III, "Critical study of thermosonic copper ball bonding," Thin Solid Films, vol. 462-463, pp.339-345, September 2004.

[4] D. S. Liu, Y. C. Chao, and C. H. Wang, "Study of wire bonding looping formation in the electric packaging process using the three-dimensional finite element method," Finite Element in Analysis and Design, vol. 40, no. 3, pp. 263-286, January 2004.

[5] Y. Liu, S. Irving, and T. Luk, "Thermosonic wire bonding process simulation and bond pad over active stress analysis," IEEE Transactions on Electronics Packaging Manufacturing, vol. 31, no. 1, pp. 61-71, January 2008.

[6] F. Y. Hung, T. S. Lui, L. H. Chen, and Y. T. Wang, "Recrystallization and fracture characteristics of thin copper wire," Journal of Materials Science, vol. 42, no. 14, pp. 5476-5482, July 2007.

[7] C. Hanga, C. Wang, M. Shi, X. Wu, and H. Wang, "Study of copper free air ball in thermosonic copper ball bonding," Proc. 6th International Electric Packaging Technology Conference, August-September, 2005, pp. 414-418.

[8] W. Y. Chang, H. C. Hsu, S. L. Fu, Y. S. Lai, and C. L. Yeh, "An investigation on heat affected zone for Au wire/Cu wire and advanced finite element wirebonding model," Proc. 3rd Microsystems, Packaging, Assembly & Circuits Technology Conference, October 2008, pp. 419-423.

[9] C. L. Yeh, Y. S. Lai, and C. L. Kao, "Transient simulation of wire pull test on Cu/low-k wafers," IEEE Transactions on Advanced Packaging, vol. 29, no. 3, pp. 631-638, August 2006.

[10] H. C. Hsu, C. Y. Hu, W. Y. Chang, C. L. Yeh, and Y. S. Lai, "Dynamic finite element analysis on underlay microstructure of Cu/low-k wafer during wirebonding," Finite Element Analysis, pp. 453-478, August 2010.

[11] S. K. Prasad, Advanced wirebond interconnection technology, Kluwer Academic Publishers, pp. 3-55, 2004.

[12] R. C. J. Wang, C. C. Lee, L. D. Chen, K. Wu, and K. S. Chang-Liao, "A study of Cu/Low-k stress-induced voiding at via bottom and its microstructure effect," Microelectronic Reliability, vol. 46, no. 9-11, pp.1673-1678, September-November 2006.